understood. Current research into the physics of wave breaking, Langmuir circulation, wave-precipitation interactions, and other surface wave phenomena will lead to improved understanding, and ultimately to useful parameterizations.

See also

Breaking Waves and Near-surface Turbulence. Bubbles. Deep Convection. Heat and Momentum Fluxes at the Sea Surface. Internal Tides. Langmuir Circulation and Instability. Penetrating Shortwave Radiation. Surface, Gravity and Capillary Waves. Three-dimensional (3D) Turbulence. Under-ice Boundary Layer. Upper Ocean Vertical Structure. Whitecaps and Foam. Wave Generation by Wind.

Further Reading

Garrett C (1996) Processes in the surface mixed layer of the ocean. *Dynamics of Atmospheres and Oceans* 23: 19–34.

Thorpe SA (1995) Dynamical processes at the sea surface. *Progress in Oceanography* 35: 315–352.

UPPER OCEAN RESPONSES TO STRONG FORCING EVENTS

L. K. Shay, University of Miami, Miami, FL, USA

doi:10.1006/rwos.2001.0159

Introduction

Strong atmospheric forcing events occur over the oceans during both summer and winter months. Cyclonically (anticyclonically) rotating wind fields around a surface low-pressure region in the Northern (Southern) Hemisphere excite an energetic ocean response. For example, winter storms and extratropical cyclones originating in the Gulf of Alaska (north-east Pacific Ocean) or over the Gulf Stream (western Atlantic Ocean) significantly impact the north-west and north-east coasts of the United States, respectively. Similarly, tropical storm formation and their subsequent development into tropical cyclones (called hurricanes in the Eastern Pacific and Atlantic Ocean basins, and typhoons in the Western Pacific Ocean) cause an energetic ocean response in these basins. In this context, the ocean's response is pronounced as manifested in the upper ocean cooling patterns that are modulated by the three-dimensional current structure excited by storms.

Observationally, studies over the past decade have demonstrated the importance of the current structure on the oceanic mixed layer (OML) thermal response. Thermal structure changes using temperature profiles and remotely sensed data acquired during hurricane conditions have been well documented. However, the oceanic current response to the surface winds has focused primarily on analytical and numerical solutions with simplifying assumptions. A key component of the current response is associated with the divergence and convergence of the OML currents that induce upwelling and downwelling regimes, respectively, in the thermocline. The wind-forced currents rotate anticyclonically with time with a period of oscillation close to the local inertial period. In addition, this wind-forced, near-inertial current vector rotates anticyclonically with depth and creates significant shear across the OML base that causes vertical mixing and upper ocean cooling. Although the current response has been thought to be confined to the upper part of the water column, fortuitous encounters of hurricanes with spatially limited current meter moorings indicate that the response extends through the thermocline to as deep as 1000 m. These data have provided a new view of the oceanic current response to storms, and have challenged theories and models concerning strongly forced conditions.

Accordingly, the ocean's current response encompasses both the directly forced or near-field region, and the evolving three-dimensional wake or far-field regime. In the near-field region, the cyclonically rotating wind field of a tropical cyclone forces the OML currents of about 1–2 $m\,s^{-1}$ to diverge from the storm track starting within one-quarter of an inertial wavelength (Λ) behind the eye, defined as the product of the storm translation speed U_h and the local inertial period (IP). This OML current divergence and net Ekman transport away from the storm track cause the upwelling of cooler water that decreases the OML depth (**Figure 1**). Over the next half of a near-inertial cycle, OML currents converge toward the storm track, causing an increase in the OML depth as warmer water is downwelled into the thermocline. This alternating cycle of upwelling and downwelling of the isotherms occurs over

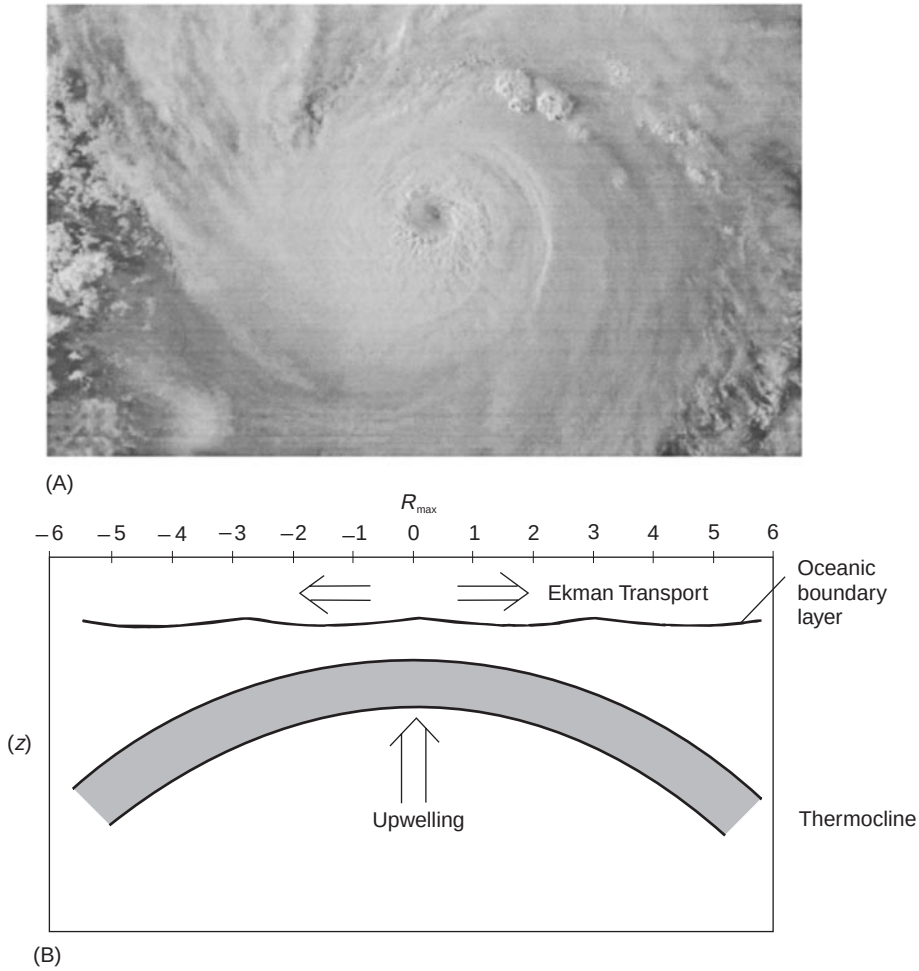

Figure 1 (A) Visible image of a well-developed hurricane. (B) Diagram of the upwelling of the isotherms (thermocline) that begins just in back of the hurricane eye relative to the radius of maximum winds. In the thermocline, there is an upward Ekman pumping velocity and a corresponding net Ekman transport away from the storm center.

distances of Λ and establishes horizontal pressure gradients that couple the wind-forced OML to the thermocline as part of a spreading three-dimensional wake.

The most apparent effect of the tropical cyclone-induced response is the marked lowering of the sea surface temperature (SST). Under strong wind-forced current regimes, SSTs, which represent the temperatures in the upper meter or less, is a proxy for the OML temperatures. Typically, OML temperatures decrease by 1–5°C to the right of the storm track at 1–2 radii of maximum winds (R_{max}) due to surface wind field asymmetries, known as the rightward bias. Although high SSTs (> 26°C) are required to maintain a tropical cyclone, maximum SST decreases and mixed layer depth increases of 20–40 m are primarily due to entrainment mixing of the cooler thermocline water with the warmer OML water. This entrainment mixing mechanism typically accounts for 70–80% of the observed SST decreases, due to either vertical current shear across the OML base or surface wind-generated turbulence. Both of these mixing mechanisms modulate the OML response which impacts storm intensity. Thus, the thermal response is a combination of upwelling along the track due to the current divergence and net Ekman transport, and mixing effects. Clearly, ocean current and its shear field is important to the strongly forced problem and this upper ocean cooling.

In the upper ocean, strong atmospheric forcing events and the isopycnal displacements induce horizontal pressure gradients and excite baroclinic near-inertial current oscillations within the thermocline. These baroclinic motions are associated with depth-dependent processes and vertical structure changes in the stratification. These forced, near-inertial waves propagate away from the storm track in the

oceanic wake as part of the geostrophic adjustment process as shown by Rossby and others. A spreading baroclinic ridge is then formed along the periphery of the upwelling and downwelling regimes that may remain in the wake for a long period of time following storm passage. For example, the near-inertial temperature and current response to hurricanes Frederic and Gloria persisted for about three weeks in the thermocline. By contrast, a cold, barotropic trough or free surface depression remains on the sea surface for several days following storm passage. This weaker barotropic response is associated with depth-independent processes due to a sloping free surface. Generally, geostrophic currents rotate cyclonically around the cold trough with weak near-inertial motions occurring along the track that radiate away quickly.

An illustrative example of this OML surface current response is evident in the surface observations from an over-the-horizon radar. During hurricane Hortense (**Figure 2**), surface currents of $1.5\,\mathrm{m\,s^{-1}}$ diverged from the storm track as part of the first upwelling cycle. The strongest response, including SST cooling of 2–3°C, occurred on the right side consistent with the rightward bias. Such spatial measurements provide context of the storm-induced response that complement *in situ* measurements such as airborne expendable current profilers. In this article, the characteristics of the oceanic response to tropical cyclones is described in terms of the applied atmospheric structure. The extensive set of oceanic current and temperature observations acquired during hurricane Gilbert provide a description of the dominant response.

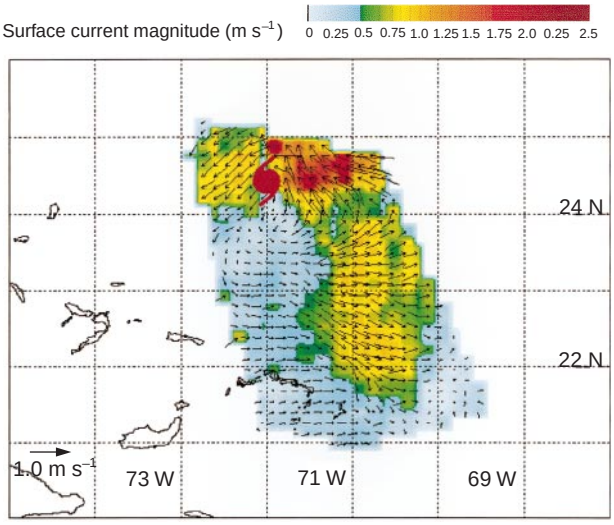

Figure 2 Over-the-horizon radar-derived surface current patterns (arrows) and magnitude (color) relative to the center of hurricane Hortense at the time of the radar image at 1600 UTC on 12 September 1996. (Adapted from Harlan and Georges, 1997.)

Atmospheric Forcing

The initial oceanic spin-up is a function of the storm parameters such as the storm translation speed (U_h), radius of maximum winds ($R_{\max}$), and the surface wind stress at 10 m ($\tau_{\max}$). The latitude of the storm is important as it sets the local planetary vorticity through the Coriolis parameter ($f = 2\Omega\sin(\phi)$, where Ω is the angular rotation rate of the Earth ($7.27 \times 10^{-5}\,\mathrm{s^{-1}}$), and ϕ is the latitude). The inverse of the Coriolis parameter is the fundamental timescale referred to as the inertial period (IP $= 2\pi f^{-1}$). Notice that the IP decreases northward, for example, at 24°N the IP is 29.5 h whereas at 35°N the IP is about 21 h. In addition, the background structure of the oceanic mixed layer depth (h), the density contrast or reduced gravity (g') between the OML and the thermocline water, thermocline thickness (b), and the phase speeds of the barotropic (c_0) and baroclinic (c_1) modes generally govern the dominant response characteristics. These air–sea parameters and their relationships to the observed response are described below.

Hurricane Gilbert

Surface winds around a surface low-pressure cell rotate cyclonically in the Northern Hemisphere as shown in **Figure 3** for the hurricane Gilbert case in September 1988. Gilbert's winds weakened as it moved into the Gulf of Mexico in a north-west direction at an average speed of $5.6\,\mathrm{m\,s^{-1}}$. Central pressures were in the 940 mbar range and maximum winds were $50–55\,\mathrm{m\,s^{-1}}$ at the primary ($R_{\max}$) of 60 km. There was a secondary wind maximum at 90 km ($1.5R_{\max}$) due in part to a contracting eye wall. These variations caused uncertainties in defining ($R_{\max}$) since it decreased from 60 km to 45 km after crossing the western Gulf of Mexico and landfalling in Mexico.

Central to the question of storm forcing and the scaling of the dominant response, is the strength of the surface wind stress and the wind stress curl defined at 10 m above the surface. Within the framework of the bulk aerodynamic formula, the wind stress is given by

$$\vec{\tau} = \rho c_d |\vec{W}_{10}| u_{10} i + v_{10} j \qquad [1]$$

where ρ is the air density, c_d is the surface drag coefficient, the magnitude of the wind ($|\vec{W}_{10}|$) is $\sqrt{(u_{10}^2 + v_{10}^2)}$, where u_{10} and v_{10} represent the wind

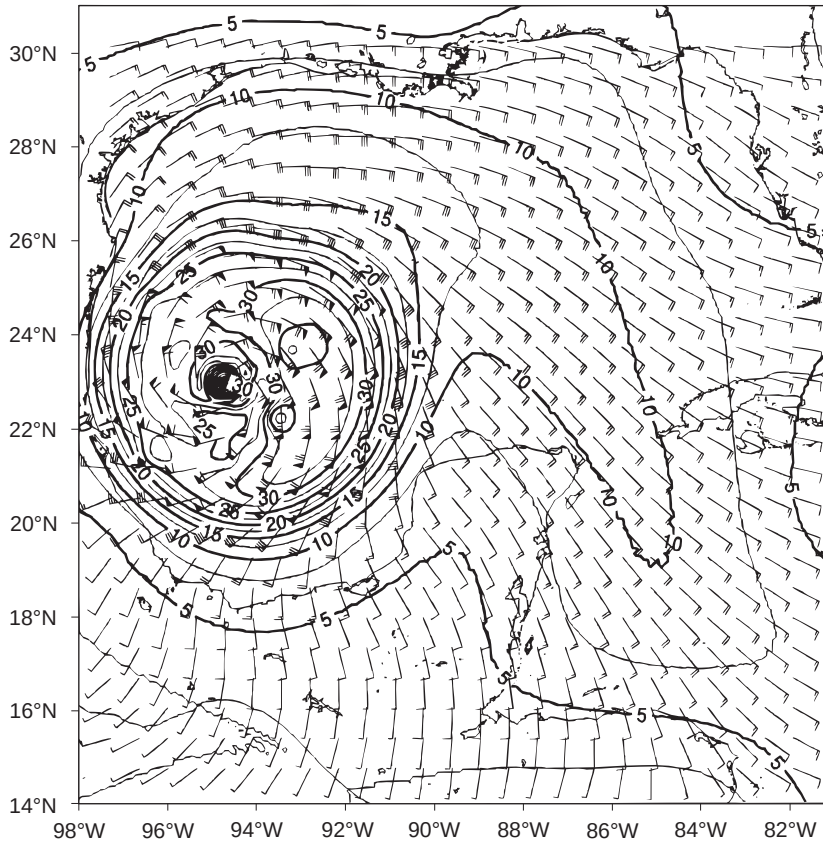

Figure 3 Surface winds derived from flight-level reduced, European Center for Medium Range Forecasting surface and buoy winds for 06 UTC, 16 September 1988. Every eighth data point from the analyzed field is plotted as a barb (in knots) with contours representing the wind magnitude in $m\,s^{-1}$. (Adapted with permission from Jacob *et al.*, 2000.)

components at 10 m above the surface in the east and north directions, respectively. In addition to a wind-speed dependence, investigations have shown the importance of sea state on the surface drag coefficient (but *see* **Heat and Momentum Fluxes at the Sea Surface**). While these studies have focused on winds of 10–25 $m\,s^{-1}$, even more uncertainty exists for c_d beyond these values. Modeling studies have emphasized the uncertainties in estimating wind stress to O(20%) under strong forcing conditions.

In hurricane Gilbert, maximum wind stress was 4.2–4.4 $N\,m^{-2}$ at R_{max} and 3.3 $N\,m^{-2}$ at $1.5R_{max}$, respectively. Central to the ocean response is the wind stress curl, defined as the spatial change in the surface wind stress vector as per [1]. The maximum value associated with the wind stress curl is within $\pm 2R_{max}$ of the eye, and causes the upper ocean currents and the net Ekman transport to diverge from the track as colder water is displaced upward (**Figure 1B**). The corresponding rate of this upward displacement of the thermocline (or Ekman pumping velocity) is proportional to the wind stress curl divided by the product of the water density and the local Coriolis parameter. Clearly, the wind stress variations demonstrate the asymmetric structure of a mature hurricane, which impacts the upper ocean structure.

An important parameter for the oceanic response is the time available for vertical mixing (L/U_h where L is the wind stress curl length scale of approximately $4R_{max}$). If this timescale is short compared to the local IP, the OML may not necessarily cool and deepen as dramatically as in the opposite case. For hurricance Gilbert, L is about 240 km, which causes this timescale to be about 12 h compared to an IP of 30 h. Thus, the ratio is 1 in 2.5 compared to 1 to 7 found in the case of hurricane Opal (1995) ($U_h = 8.5\,m\,s^{-1}$) for strong and weak upper ocean cooling regimes, respectively.

Coordinate System and Scales

Based on Gilbert's translation speed and the local IP, the predicted wavelength (Λ) is estimated to be 586 km with an uncertainty of ± 30 km (**Table 1**). Observed profiles are then placed into a

Table 1 Air–sea parameters, nondimensional numbers and scales in hurricane Gilbert based upon Price scaling arguments. The maximum stress represents the symmetric part of the wind stress field based on a fit to a Rankine vortex for the purpose of scaling[a]

Parameter		
Radius of maximum winds (km)	R_{max}	60
Maximum wind stress ($N\,m^{-2}$)	τ_{max}	3.5
Speed of the hurricane ($m\,s^{-1}$)	U_h	5.6
Wavelength (km)	Λ	586
First mode phase speed ($m\,s^{-1}$)	c_1	2.8
First mode deformation radius (km)	α_n^{-1}	46
Inertial period (day)	IP	1.25
Reduced gravity ($m\,s^{-2}$)	g'	2.86×10^{-2}
Mixed layer depth (m)	h	35
Thermocline scale (m)	(b)	200
Nondimensional numbers		
Froude number (Fr)	U_h/c_1	2
Nondimensional storm speed (S)	$(U_h/2R_{max}f)$	1.04
Scales		
Wind-driven velocity (V_{is})	$\tau_{max}R_{max}/\rho_0 hU_h$	$1.07\,m\,s^{-1}$
Thermocline velocity (V_{th})	h/bV_{is}	$0.22\,m\,s^{-1}$
Isopycnal displacements (η_s)	$\tau_{max}/\rho_0 f U_h$	13 m
Geostrophic velocity (V_{gs})	$g'\eta_s/fR_{max}$	$0.11\,m\,s^{-1}$

[a]Adapted from Shay et al. (1998).

storm-coordinate system relative to the position of the storm's eye, allowing along-track distance to be converted into time by assuming a steadily moving storm. This transformation is important to an understanding of the evolving oceanic response in along- and cross-track directions normalized by Λ and R_{max}, respectively.

In understanding the wind forcing dynamics on the OML response, the ocean currents rotate anticyclonically with time where the period of oscillation is close to the local inertial period. As these wind-forced inertial currents have frequencies that are close to, but slightly higher than, the local inertial frequency by 1–20%, they are known as near-inertial motions. This shift in frequency above f is required for energy to propagate vertically from the wind-forced OML into the thermocline. Based on Gilbert's air–sea parameters, the frequency shift was found to be about 4% of f, which is within the envelope of expected values. Other important scales based on the air–sea parameters are listed in **Table 1** and provide representative values to compare observational and numerical data sets.

Initial Ocean Structure

An important parameter governing the oceanic response is the phase speed of waves due to oceanic density changes between the OML and the thermocline. One possible modeling approach is to use a two-layer model, which allows for both barotropic and baroclinic modes. The barotropic mode is referred to as the external mode whereas the baroclinic mode is the first internal mode. However, when the vertical density structure is continuous (density stratification varies continuously with depth), an infinite set of baroclinic modes is permissible including the barotropic mode associated with the time- and space-dependent variations in the free surface. This is the rationale for treating barotropic and baroclinic modes separately in numerical models.

Two-Layer Approach

In a two-layer flow regime, the phase speed of the first baroclinic mode (c_1) is

$$c_1^2 = \frac{g(\rho_2 - \rho_1)h_1 h_2}{\rho_2(h_1 + h_2)}, \qquad [2]$$

where ρ_1 is the density of the upper-layer of depth h_1, and ρ_2 is the density in the lower layer of depth h_2 where $\rho_2 > \rho_1$. In the coastal ocean, phase speeds range from 0.1 to $0.5\,m\,s^{-1}$, whereas in the deep ocean, this phase speed lies between 1 and $3\,m\,s^{-1}$ depending on the density contrast between the two layers. The external or barotropic mode has a phase speed $c_0 = \sqrt{(gH)}$ where H represents the total depth $(h_1 + h_2)$. Typically, the phase speed for the barotropic mode is O(100) times larger than the first baroclinic mode phase speed.

An important nondimensional number for estimating the expected baroclinic response depends on the ratio of the translation speed to the first baroclinic mode phase speed (U_b/c_1). If this ratio is less than unity (i.e., stationary or slowly moving storms), large geostrophically balanced currents are generated by the wind stress curl causing an upwelling of cooler water induced by Ekman transport from the storm track. If this ratio exceeds unity, the ocean response is predominantly a baroclinic process associated with upwelling and downwelling of the isotherms and the spreading wake of forced, near-inertial motions.

The predominance of a geophysical process depends on the deformation or Rossby radius of the first baroclinic mode (α^{-1}) defined as the ratio of the first mode phase speed (c_1) to the local Coriolis parameter (f). In the coastal regime, the deformation radius is O(5–10 km), but further offshore beyond the shelf break, it increases to 20–50 km due to larger phase speeds. For observed scales exceed-

ing the deformation radius, rotational effects tend to dominate the oceanic dynamics where timescales are equal to or greater than the IP. For the strongly forced case, rotational effects dominate the oceanic response.

Ocean Stratification and Vertical Modes

A representative profile from the western Gulf of Mexico is used to determine the buoyancy frequency profile and the vertical mode structure (**Figure 4**). The maximum buoyancy frequency, N (where $\bar{N}^2(z) = (g_1/\rho_0)(\partial\bar{\rho}/\partial z)$, with N in radians s^{-1}) is about 12 cycles per hour (cph) located between the OML (40 m) and the top of the thermocline. Below this maximum buoyancy frequency, a region of buoyancy frequencies > 3 cph are concentrated in the seasonal thermocline over an approximate scale (b) of 200 m (see **Table 1**) that exponentially decays with depth and approaches 0.1 cph at 1000 m.

The modal structure can be thought of as a vibrating string with both ends fixed. By imposing an external force on the string, the string will be distorted into several different positions or modes. In a similar way, the background oceanic stratification (i.e., **Figure 4**) supports an infinite set of baroclinic modes between rigid (fixed) boundaries at the ocean's surface and bottom. Key parameters from solving the normal mode equation for the buoyancy frequency profile are listed in **Table 2**. For near-inertial motions baroclinic mode number (n) increases, the phase speeds, horizontal wavelengths, deformation radii for each mode all decrease while the corresponding timescales increase as described below.

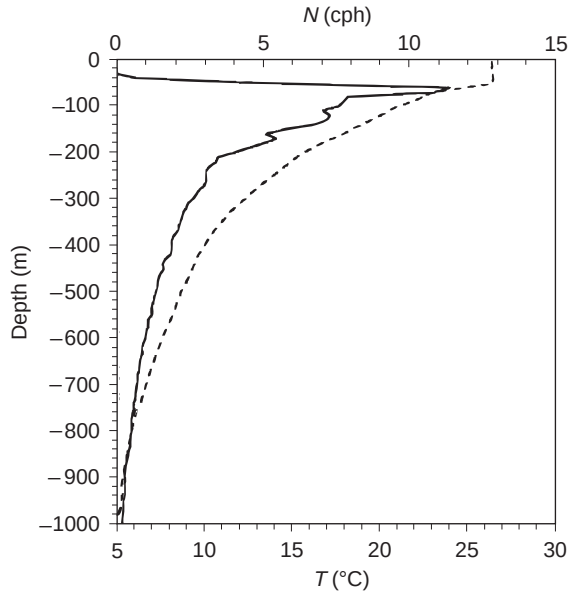

Figure 4 Buoyancy frequency (N, solid line) and corresponding temperature profile (T, dashed line) from a conductivity, temperature and depth profiler station in the western Gulf of Mexico at about 23°N. (Adapted with permission from Shay *et al.*, 1998.)

Table 2 Phase speed (c_n), deformation radius (α_n^{-1}), wavelengths (λ_n), equivalent forcing depth ($\int_{-D}^{0}\phi_{nz}^2 dz$) and t_n for $N(z)$ in the western Gulf of Mexico (**Figure 5B**) estimated for each baroclinic modes

Mode n	C_n ($m\,s^{-1}$)	α_n^{-1} (km)	λ_n (km)	$\int_{-D}^{0}\phi_{nz}^2 dz$ (m)	t_n IPs[a]
1	2.8	46	283	119	2.1
2	1.79	29	180	287	6.5
3	1.23	21	116	449	15
4	0.89	15	89	828	27

[a]IPs, inertial periods.

To illustrate this vertical modal structure, the normalized vertical (ϕ_n) and horizontal velocity eigenfunctions ($d\phi_n/dz$) for the first four baroclinic modes are estimated from the buoyancy profile (**Figure 5**). For the first baroclinic mode, the largest horizontal velocity is in the OML and is the most energetic mode. As mode number increases, larger structural values tend to be displaced downward towards the thermocline. In fact, higher-order modal eigenfunctions not only increase relative to their OML value, but their amplitudes contain more vertical structure that contribute to larger current differences (i.e., current shears). Thus, this relatively simple ocean structure provides insights into the predominance of the low-mode response to strong forcing events. This is useful in isolating physical processes and designing numerical modeling experiments.

Based on their low baroclinic mode characteristics, there is a fundamental timescale for the phase of each baroclinic mode to separate it from the wind-forced OML when the scale of the wind stress (typically $2R_{max}$), exceeds the deformation radius associated with the first baroclinic mode (O(40 km)). It has been shown that the baroclinic timescale required for a phase difference of $\pi/2$ to develop for each baroclinic mode (n) in the OML is

$$t_n = \frac{\pi f}{K^2 c_n^2} \qquad [3]$$

where K^{-1} represents the horizontal wavenumber of the wind stress associated with the storm. As mode number increases, the baroclinic timescale increases and the lower modes separate from the OML faster than higher-order modes. These timescales may also

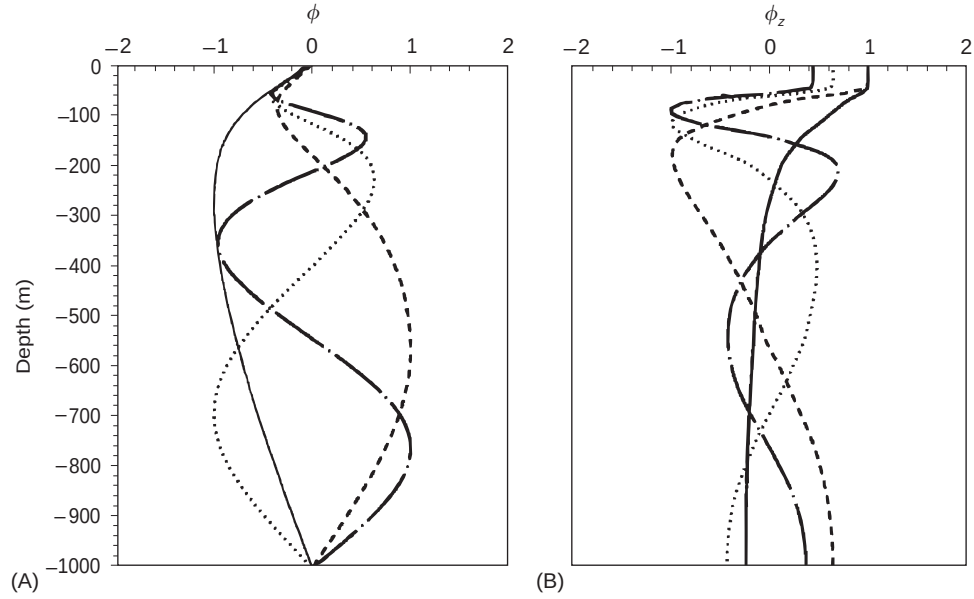

Figure 5 Amplitudes of the (A) vertical (ϕ_n) and (B) horizontal velocity ($d\phi_n/dz$) eigenfunctions from a conductivity, temperature and depth profiler station as in **Figure 4** for 1st (solid), 2nd (dashed), 3rd (dotted) and 4th (chain-dashed) baroclinic modes. (Adapted with permission from Shay *et al.*, 1998.)

represent the onset of rapid vertical energy propagation from the OML into the thermocline.

Current and Temperature Response

Baroclinic Response

Sanford and colleagues pioneered a new era of acquiring high-resolution ocean current and temperature profiles from airborne expendable current profilers which could be deployed in strong forcing regimes. This profiler is deployed from an aircraft at altitudes of 1500–2500 m. As the profiler is jettisoned from the aircraft, a parachute opens as it falls towards the ocean surface. Once in the ocean, a seawater battery causes a flotation device to inflate with a radio frequency antenna. Within 30 s, the profiler is released from its airborne canister and is attached to the surface unit by thin copper wire. The surface unit then transmits data to the aircraft through the radio-frequency link as the profiler descends at $4.5\,m\,s^{-1}$ through the water column. This current measurement is based on the principle of motionally induced voltage differences between two electrodes, and provides accurate baroclinic current measurements at intervals of about 2–3 m with root mean square errors of $1–2\,cm\,s^{-1}$ relative to an unknown, but constant, depth-independent flow. These measurements provide unprecedented, three-dimensional snapshots of the ocean current and temperature structure to 1500 m in the directly forced regime. In hurricane environments, baroclinic currents in the OML range from 1 to $1.5\,m\,s^{-1}$ after removal of the surface-wave induced orbital velocities associated with low-frequency swell (i.e., 10 s period surface waves). These profilers have been successfully deployed in both storm and nonstorm environments with success rates of 80–95%.

One approach in understanding these profiler measurements in storms is through the forced dynamical modes to simulate the observed three-dimensional velocity field. The free mode problem is first solved subjected to rigid boundary conditions for a given buoyancy frequency profile ($\bar{N}(z)$). After calculating these baroclinic modes, the linear equations of motion are expanded in terms of the baroclinic modes for the vertical velocities and densities (ϕ_n) and horizontal velocities and pressures ($d\phi_n/dz$) (shown in **Figure 5A,B**). This expansion leads to the projection of the baroclinic modes on the surface wind stress

$$X_n, Y_n(x,y) = \frac{\tau^x, \tau^y(x,y)}{\rho_0 \int_{-D}^{0} \phi_{nz}^2 dz} \qquad [4]$$

where $d\phi_n/dz = \phi_{nz}$ (**Figure 5B**) and the mixed layer depth (h) is replaced by an equivalent forcing depth ($\int_{-D}^{0} \phi_{nz}^2 dz$) (**Table 2**). Since equivalent forcing depth increases with mode number, this projection decreases the modal wind stress, which is the rationale for the low-mode dominance of the current response.

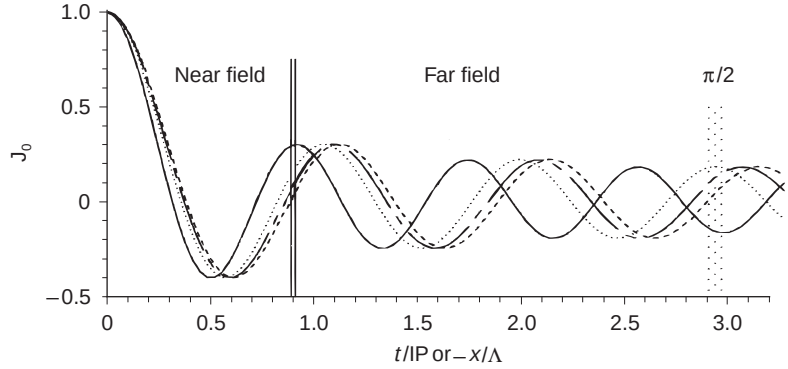

Figure 6 Amplitudes of the Bessel function for normalized time (time divided by the inertial period, IP) or distance ($-x\Lambda^{-1}$) for the 1st (solid), 2nd (dotted), 3rd (dashed) and 4th (chain-dashed) baroclinic modes. Notice the point (≈ 2.9 IP) where a $\pi/2$ phase difference develops between the first and second baroclinic modes which is about 2.1 IP from the boundary between the near and far fields. (Adapted with permission from Shay *et al.*, 1998.)

For the three-dimensional hurricane-induced response, the horizontal structure coefficients are found by convolving a Bessel function (J_o) with the modal wind stress forcing pattern as in eqn [4]. A Bessel function is a special function in mathematical physics dealing with circular features such as hurricanes. In this context, Bessel function amplitudes for the first four baroclinic modes decay rapidly over the first 0.5 IP following Gilbert's passage (**Figure 6**). For example, the first baroclinic mode decreases from 1.0 to -0.4 within 0.5 IP, and subsequently increases to 0.3 after 1 IP. Given this behavior, the transition between the near-field and far-field regimes may occur between 0.75 and 1 IP following passage. As time evolves, the first baroclinic mode separates from other modes in the OML after about 2 IP (≈ 2.9 IP), and is directly out of phase with the higher-order modes by 3 IP. These predicted timescales will be shown to agree reasonably well with the observed near-inertial current variability.

Mixed Layer and Thermocline Current Response

By summing baroclinic modes (i.e., a product of the horizontal coefficient and the vertical structure function for each baroclinic mode), OML horizontal velocities can be estimated (**Figure 7**). These indicate a net horizontal divergence and convergence of an anticyclonically rotating current with a maximum speed of 1.2 m s^{-1} between the hurricane track and $R_{\max}$. This slight rightward displacement of the maximum response is due to the asymmetry of the imposed wind field. The spreading of the velocity field with time (or equivalently along-track distance) in the wave wake, fills a wedge following a $\tan^{-1}[(u_b^2/c_i) - 1]^{1/2}$ dependency. At the OML base, the maximum upward vertical velocity is 0.7 cm s^{-1} during the upwelling phase due to the OML current divergence (**Figure 7A**). Maximum horizontal velocities at the OML base are about 0.82 m s^{-1} (not shown). Over the next half cycle, vertical velocities are downward as the OML currents converge towards the storm track. In the thermocline (**Figure 7B**), currents are reduced to a value of about 0.20 m s^{-1} that agrees well with the predicted thermocline velocity scale (listed in **Table 1**). This result suggests that the initial ocean response scales well with storm forcing variables (U_h, $\tau_{\max}$, and $R_{\max}$). Since the thermocline current is opposite to the OML flow, current vector also rotates anticyclonically with depth. The corresponding vertical velocities of 0.2 cm s^{-1} are in the same sense as those across the OML base (**Figure 7B**).

Over the first 1.7 IP following the storm, a large fraction of the residual current variance (up to 78%) is described by wind-forced near-inertial motions (**Figure 8**) based upon linear physics. Notice the consistencies between the residual and near-inertial profiles where maximum amplitudes are 0.9 (1.1 m s^{-1}) in the OML (**Figure 8B**). By removing geostrophic velocity profiles, root mean square amplitudes of the unresolved currents decrease from 15 cm s^{-1} in the OML, to 5 cm s^{-1} in the thermocline, and to 2 cm s^{-1} at depth. The simulated current structure based on four modes is consistent with the observed current profiles (**Figure 8C**). Generally, correlation coefficients between near-inertial and simulated profiles exceed 0.7 for the first six profiles encompassing both the Storm and Wake 1 experiments. During Wake 2, correlation coefficients range from 0.4 to 0.7, except for the profile after 2.9 IP due to the phasing between the first baroclinic mode and other baroclinic modes in the OML as suggested in **Figure 6**.

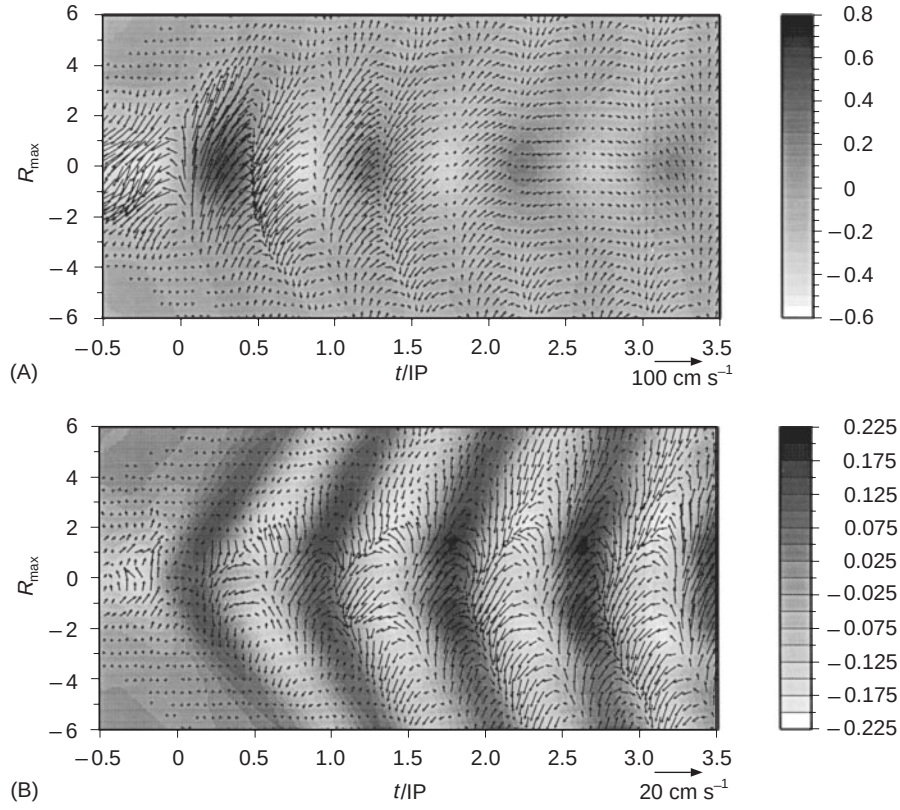

Figure 7 Simulated (A) mixed-layer current (arrows) and vertical velocity (shaded) at ocean mixed layer (OML) base, and (B) thermocline current and vertical velocity structure from a sum of the first 10 baroclinic modes. Maximum OML and thermocline currents are 1.20 and 0.22 m s^{-1}, respectively. Maximum vertical velocities, contoured at an interval of 0.05 cm s^{-1}, are 0.7 and 0.25 cm s^{-1}. Along-track and cross-track distances are scaled in terms of Λ (586 km) and R_{max} (60 km). The horizontal scale is time divided by one inertial period.

Mixed Layer Thermal Response

Observations reveal on OML temperature decrease of 3.5–4°C to the right of hurricane Gilbert's track associated with a deeper layer of 70 m. The spatial evolution of the OML response indicates a near-inertial, wave-like pattern between the track and $3-4R_{max}$ (**Figure 9**). Temperature gradients between the pool of cooler water and a warm core ring (WCR) located beyond $4R_{max}$ are 3°C over a 50 km distance, indicating that there was a potential for strong thermal advection by the mesoscale ocean current field.

To understand this effect, the terms in the conservation of heat expression are diagnosed from the grids of analyzed data in the OML. That is, various terms are estimated in the expression to assess the relative importance of each process in the observed OML cooling pattern. One of the most important terms is the entrainment heat flux, representing the active exchange of heat between the OML and the thermocline water. This term has two components for strongly forced motions: stress-induced turbulent mixing due to surface wind stress; and current shear ($\delta\upsilon$) at the OML base associated with shear instabilities at low Richardson numbers.

Vertical Mixing

As shown in **Figure 10**, structural measurements from both inside and outside a WCR demonstrate the marked thermal contrast in the forced upper oceanic layers. Directly along the track (**Figure 10A**), the OML depth is about 40 m with currents of about $0.6\,V_{is}$, where V_{is} represents the scaled wind-driven current (**Table 1**). At the base of the OML, these currents decrease and reverse direction, which creates current shear of $10^{-2}\,s^{-1}$. This shear lowers the gradient Richardson number, defined as $R_i = \bar{N}^2/\bar{V}_z^2$, to below the critical limit of 0.25. This forces the warm and cool water to mix resulting in a deeper OML. Outside the WCR, the OML depth is 40 m, and strong stratification occurs in the thermocline ($\bar{N} \approx 15$ cph). By contrast, the isothermal layer depth in the WCR (**Figure 10B**) is about

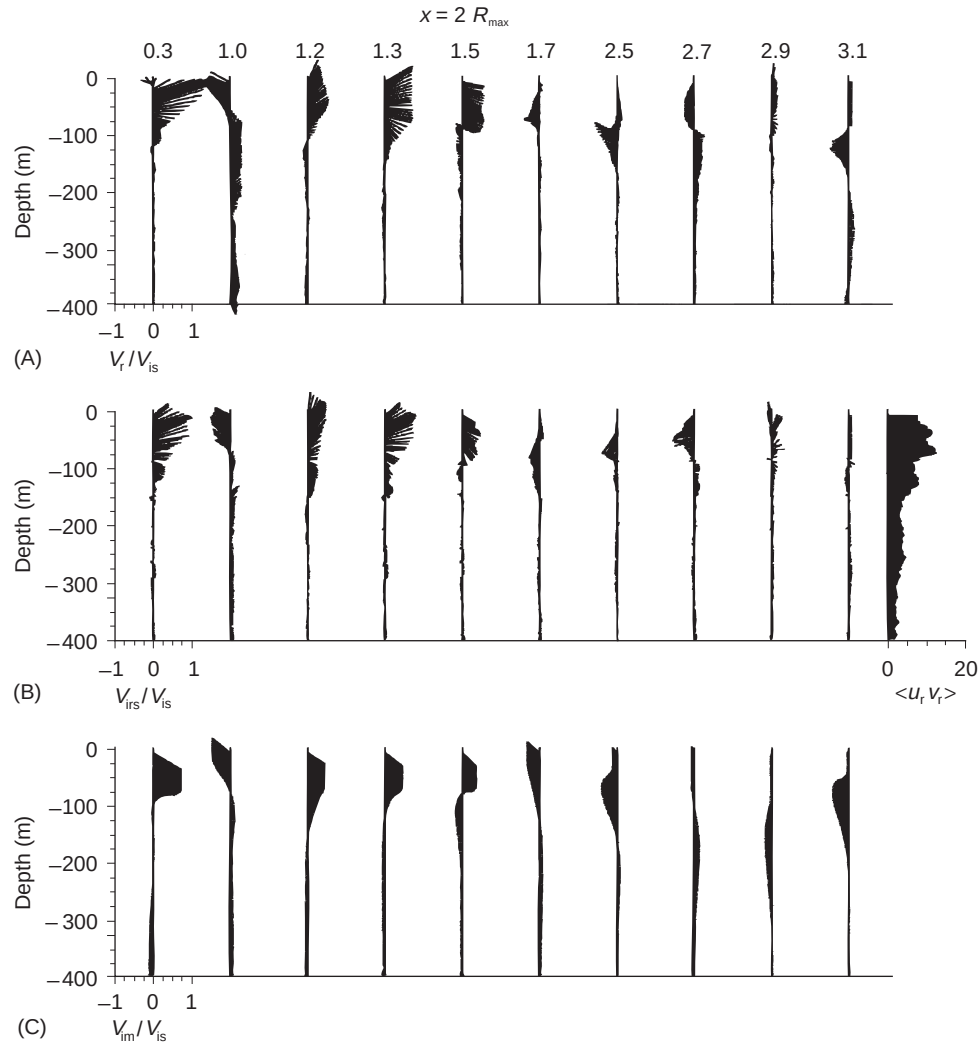

Figure 8 (A) Residual (observed-geostrophic) velocities, (B) near-inertial velocity profiles from a least-squares model (including averaged rms velocity differences in $cm\,s^{-1}$) and (C) simulated velocity structure for the four-mode model in the upper 400 m at $2R_{max}$. Velocities are normalized using $1.07\,m\,s^{-1}$ based on Price scaling, and time of each airborne expendable current profiler deployment is scaled by the inertial wavelength (Λ = storm translation speed $\times$ inertial period) relative to the storm center.

60 m with fairly weak stratification ($\bar{N} \approx 6$ cph). In the warm subtropical water, salinity variations contribute to density and hence buoyancy frequency profiles.

The deeper isothermal layer between 60 and 170 m is of central importance in the WCR and the storm itself. Warmer water with temperatures approaching 26°C extend to greater depths than in the usual case in the Gulf common water (130 m versus 50 m). These higher temperatures at depth have a significant influence on the heat content contrast between the two water masses. Outside the WCR, the heat content is less than $60\,kJ\,cm^{-2}$ compared to about $125\,kJ\,cm^{-2}$ within the WCR during the storm relative to 26°C even after some initial mixing. It has been shown that about $16\,kJ\,cm^{-2}\,day^{-1}$ is needed to maintain the storm. More importantly, vertical shear at the base of this isothermal layer ($\approx$160 m) is insufficient to induce any further layer cooling by vertical mixing as the R_i exceeds 0.25. In this context, this deep isothermal structure provides more heat for atmospheric disturbances by enhanced air–sea surface fluxes as shown in Opal.

OML Heat Budget

From the analyzed grids of profiler data, the OML heat balance was assessed during hurricane Gilbert. Geostrophic advection of the thermal gradient has a maximum value of $-0.7°C\,day^{-1}$ in the WCR region ($4 - 5R_{max}$). Because of the positive gradients

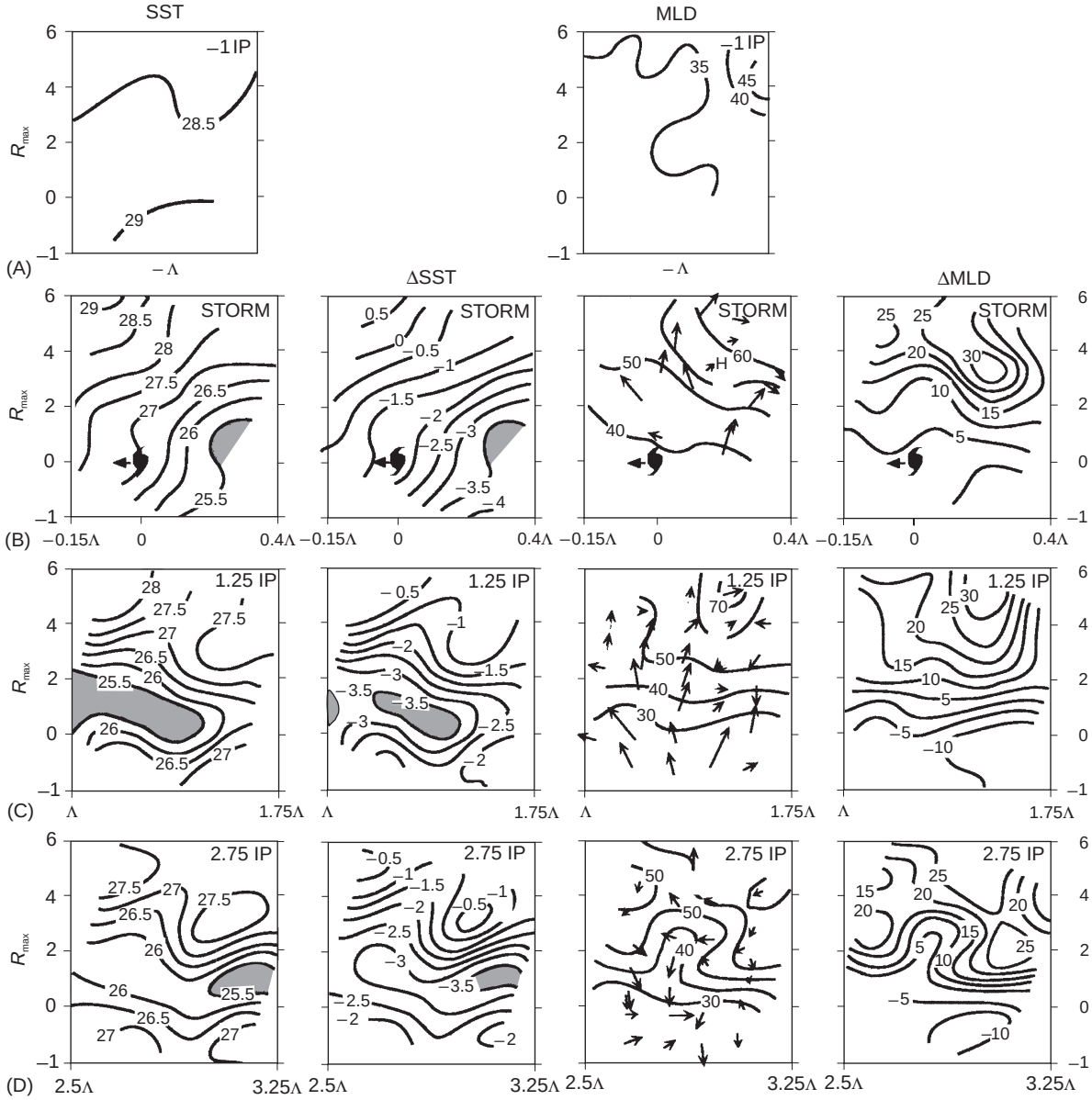

Figure 9 Objective analysis of sea surface temperatures (SSTs) (°C) and mixed-layer depth (MLD) (m). The left two columns are SSTs and ΔSSTs and the right two columns show MLDs and ΔMLDs for (A) Prestorm, (B) Storm, (C) Wake 1 and (D) Wake 2 in hurricane Gilbert. The ΔSST and ΔMLD represent changes in the SST and MLD, estimated by removing prestorm values (panel A) from the storm, Wake 1, and Wake 2 (panels B, C, D) from each snapshot. Panels are storm-coordinate systems as in **Figure 7**. (Reproduced from Shay *et al.*, 1992.)

between the track and the WCR, prestorm geostrophic velocities transport cooler water near the storm track toward the WCR in the front half of the storm, and WCR water is displaced towards the track in the rear half (**Figure 11A**). Near-inertial advection has maximum values close to the storm track because of the larger near-inertial velocities (**Figure 11B**). However, the maximum OML cooling is due to entrainment heat flux; that is, the local rate of temperature change due to entrainment heat flux ranges from -17 to $-30\,^{\circ}\mathrm{C\,day^{-1}}$ that depends on the entrainment velocity because of a near-constant MLD and stratification close to the storm track (**Figure 11C**). For example, the entrainment flux predicted by shear instability has negligible entrainment in the WCR where geostrophic advection dominates its heat balance. In addition, the local maxima tend to be enhanced in the

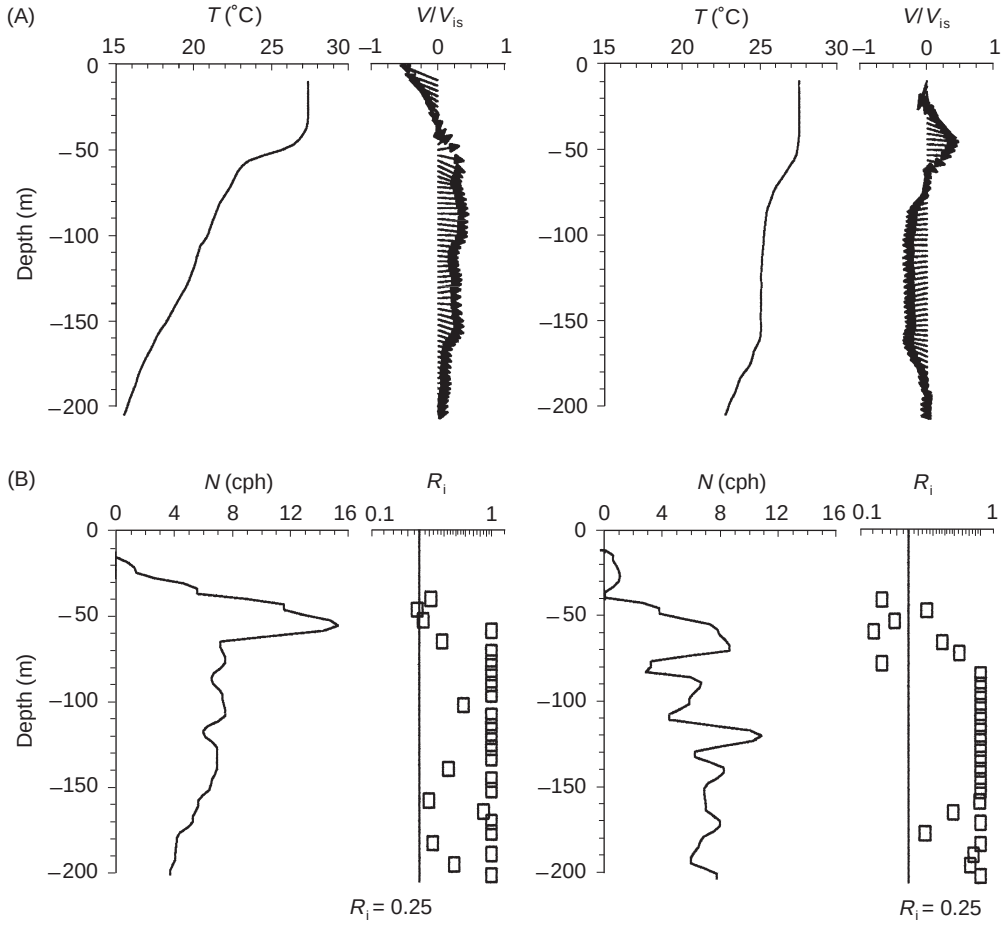

Figure 10 Vertical structure analysis of two velocity, temperature, and density profiles from the hurricane Gilbert measurements outside the warm core ring (WCR) (left panels) and inside the WCR (right panels) for (A) temperature (°C) and residual velocity (observed-geostrophic) normalized by the scaled wind-driven velocity of 1.07 m s^{-1}, and (B) buoyancy frequency (cph) and gradient Richardson number where the solid line depicts the critical value of 0.25. (Reproduced with permission from Shay *et al.*, 2000.)

entrainment heat flux term corresponding to the local wind maxima (**Figure 11D**). Surface wind stress-induced entrainment is $-4°\mathrm{C\,day^{-1}}$ away from the track due to hurricane Gilbert's broad wind field. Although the geostrophic advection is quasi-steady over storm-forcing scales, this entrainment heat flux is intermittent at this rate to produce the observed OML cooling. Despite comparable maxima of entrainment heat flux by these processes, the OML heat budget differs significantly as indicated by the average rate of cooling over the domain due to entrainment fluxes of shear- and surface-induced entrainment of $-2°\mathrm{C\,day^{-1}}$ and $-5°\mathrm{C\,day^{-1}}$, respectively. Finally, the maximum cooling rate due to surface heat loss to the atmosphere is $-0.7°\mathrm{C\,day^{-1}}$. The pattern of this surface heat flux follows the wind speed as predicated on the bulk aerodynamic formula (**Figure 11E**). The important result here is that geostrophic advection of thermal gradients is as large as the surface heat flux term in the OML heat budget. In other words, the WCR played an important role on the OML heat budget during Gilbert's passage.

Concluding Remarks

The salient features of the ocean's current and temperature response to hurricane forcing has been reviewed using observations, theories and models in the directly forced and evolving wake regimes. The upper ocean's temperature response is significantly influenced through the divergent and convergent current regimes by a time-dependent Ekman pumping on the thermocline, and to a much greater extent on the vertical current shear across the OML base to the right of the track. Divergent and convergent currents occur over near-inertial timescales or alternatively along-track wavelengths. This forced current pattern causes upwelling and downwelling

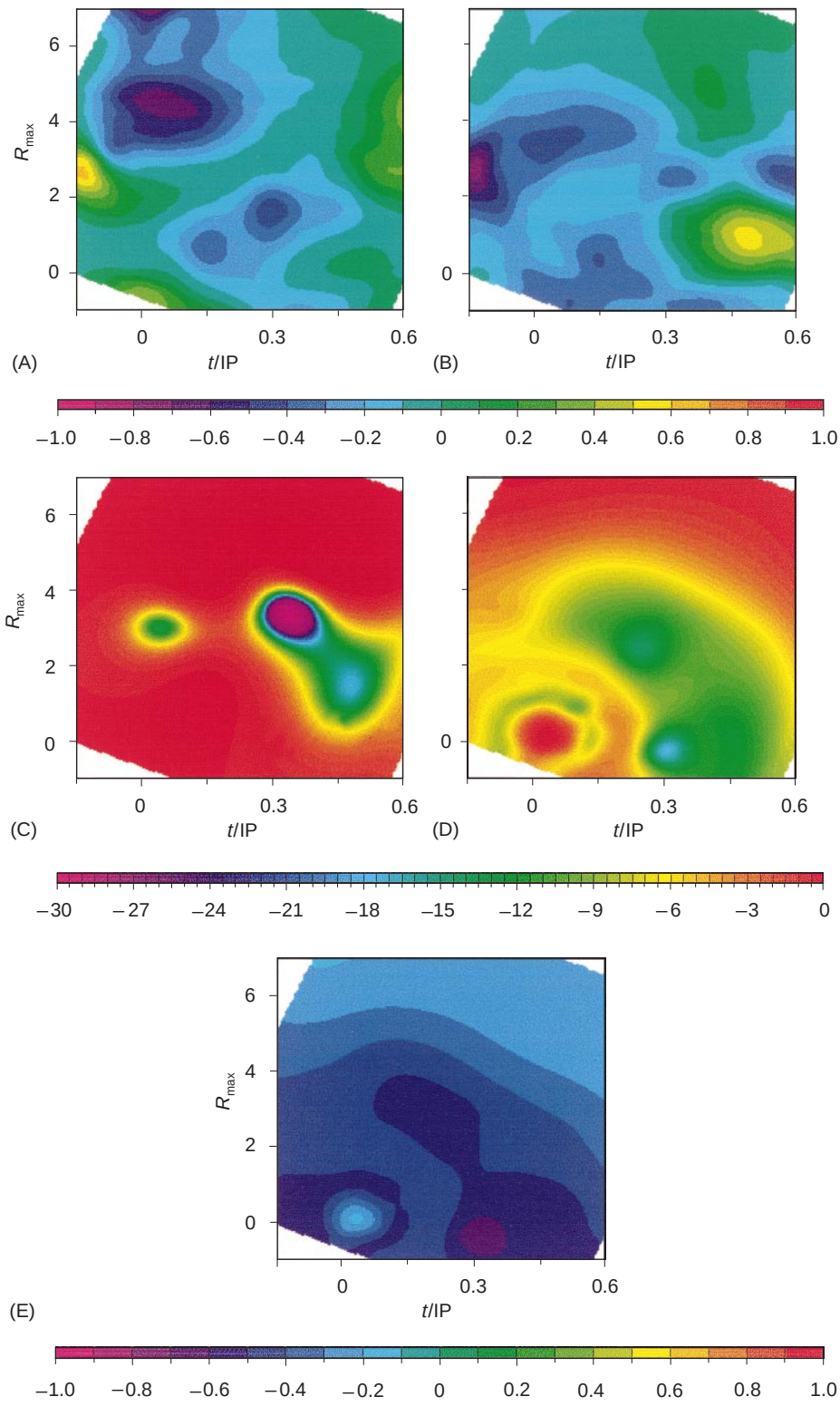

Figure 11 Ocean mixed layer heat budget during the Storm experiment in °C day^{-1}. (A) Geostrophic advection, (B) near-inertial advection, (C) entrainment heat flux by shear stability, (D) entrainment heat flux by surface stress and (E) surface heat flux. (Reproduced with permission from Jacob *et al.*, 2000.) The horizontal scale is time divided by one inertial period.

of the isotherms. Thus, a large fraction of this near-inertial current response excited by tropical cyclones is baroclinic driven by the wind stress and its curl. In this context, low-order baroclinic modes are more energetic in terms of forced near-inertial current whereas the high-order modes dominate the shear field.

The SST and OML changes depend on the intensity and speed of the tropical cyclone and the underlying ocean stratification. The rightward bias of the maximum SST and OML response has been observed and modeled due primarily by vertical current shear across the base of the OML associated with near-inertial processes. Shear instabilities lower the Richardson number to less than criticality, and cause the OML and thermocline water to mix. When the upper bounds of these cooling events are achieved, the surface fluxes feeding the storm begin to decrease which reduces intensity. This is known as the negative feedback that usually refers to processes beginning in back of the storm's eye.

Further Research

A new and promising avenue of research is beginning to focus on the upper ocean's role on intensity change and the variability in the air–sea fluxes. Since winds begin to mix the thin 'skin' layer of SST well in front of the storm, the storm actually senses the heat from the OML. The thermal skin temperatures will then represent the temperatures of the OML. For example, the *in situ* measurements in hurricane Opal indicate that in the WCR, the SST, which is a proxy for OML temperature under strong wind conditions, only cooled by 0.5°C where rapid intensity changes occurred. In this framework, the ocean provides more positive feedback simply because the upper ocean does not significantly cool in regions of deep, warm OML such as fronts and WCRs. The oceanic heat content relative to 26°C is more important than an SST in a strongly forced problem.

To illustrate this point, oceanic heat content distribution based on recent airborne oceanographic

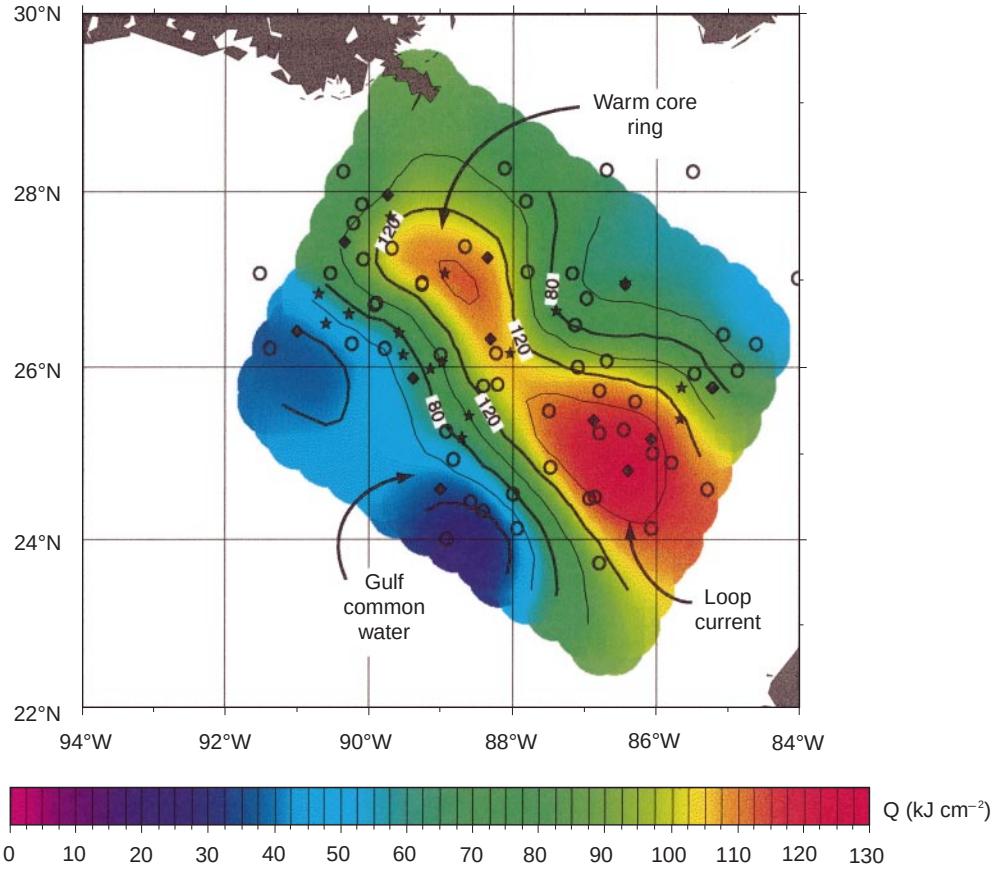

Figure 12 Ocean heat content (color) and isotherm depth of the 26°C water (contour) based on airborne expendable current profilers (star), airborne expendable conductivity, temperature and depth recorders (diamond), and airborne expendable bathythermographs (circle) deployed in the eastern Gulf of Mexico in August 1999 from a National Oceanographic and Atmospheric Administration WP-3D research aircraft flight in support of the Hurricane Research Division's mission.

measurements from the NOAA WP-3D in August 1999 indicates a striking contrast between the WCR and Loop Current and the Gulf common water (**Figure 12**). In this deep warm reservoir, the isotherm depth of the 26°C water is 120–130 m where heat content is a maximum of 130 kJ cm^{-2}. This is a factor of 8–10 times larger than is necessary to maintain a tropical cyclone. Notice that the WCR north west of the Loop Current also contains the same oceanic characteristics. By contrast, the Gulf common water (lower left) has isotherm depths of 40 m with heat content of less than half that of the Loop Current and WCR system. This implies that the warm frontal boundary currents and rings will influence the air–sea fluxes feeding the storm that may cause a storm to intensify if atmospheric conditions are favorable. In addition to using airborne measurements, this area of research also utilizes satellite-based radar altimeters in assessing and monitoring upper ocean heat content. From a practical standpoint, accurate monitoring of these processes and the ensuing air–sea fluxes are crucial to improve forecasts of storm intensity within 36 h of landfall. Thus, this new avenue of research has applications to the operational community in providing forecasts for landfalling storms where warm subtropical water is located close to the coast.

See also

Expendable Sensors. Heat and Momentum Fluxes at the Sea Surface. Ocean Circulation. Wind Driven Circulation.

Further Reading

Donelan MA (1990) Air–sea interaction. *The Sea: Ocean Engineering Series* 9: 239–292.

Gill AE (1982) *Atmosphere–Ocean Dynamics*. New York: Academic Press.

Gill AE (1984) On the behavior of internal waves in the wakes of storms. *Journal of Physical Oceanography* 14: 1129–1151.

Ginis I (1995) Ocean response to tropical cyclone. In: Elsberry RL (ed.) *Global Perspectives of Tropical Cyclones*, pp. 198–260. Geneva, Switzerland: Elsberry, World Meteorological Organization, WMO/TD-693.

Harlan J and Georges TM (1997) Observations of hurricane Hortense with over the horizon radars. *Geophysics Research Letters* 24(14): 3241–3244.

Jacob SD, Shay LK, Mariano AJ and Black PG (2000) The 3-dimensional mixed layer response during hurricane Gilbert. *Journal of Physical Oceanography* 30: 1407–1429.

Leipper DF and Volgenau D (1972) Hurricane heat potential of the Gulf of Mexico. *Journal of Physical Oceanography* 2: 218–224.

Price JF, Sanford TB and Forristall GZ (1994) Forced stage response to a moving hurricane. *Journal of Physical Oceanography* 24: 233–260.

Sanford TB, Black PG, Haustein J *et al.* (1987) Ocean response to hurricanes. Part I: Observations. *Journal of Physical Oceanography* 17: 2065–2083.

Shay LK (1994) Oceanic response to tropical cyclones. In: Majumdar SK, Miller EW, Forbes GS, Smaltz PF and Panah AA (eds). *The Oceans: Physical–Chemical Dynamics and Human Resources*, pp. 124–145. Easton, PA: Pennsylvania Academy of Sciences.

Shay LK, Black PG, Mariano AJ, Hawkins JD and Elsberry RL (1992) Upper ocean response to hurricane Gilbert. *Journal of Geophysical Research* 97(12): 20227–20248.

Shay LK, Mariano AJ, Daniel Jacob SD and Ryan EH (1998) Mean and near-inertial ocean current response to hurricane Gilbert. *Journal of Physical Oceanography* 28: 858–889.

Shay LK, Goni GJ and Black PG (2000) Effects of a warm oceanic feature on hurricane Opal. *Monthly Weather Review* 128(5): 1366–1383.

UPPER OCEAN TIME AND SPACE VARIABILITY

D. L. Rudnick, University of California, San Diego, USA

doi:10.1006/rwos.2001.0151

Introduction

The upper ocean is the region of the ocean in direct contact with the atmosphere. Air–sea fluxes of momentum, heat, and fresh water are the primary external forces acting upon the upper ocean (*see* **Heat and Momentum Fluxes at the Sea Surface; Evaporation and Humidity; and Wind and Buoyancy-forced Upper Ocean**). These fluxes impose the temporal and spatial scales of the overlying atmosphere. The internal dynamics of the ocean cause variability at scales distinct from the forcing. This combination of forcing and dynamics creates the tapestry of oceanic phenomena at timescales ranging from minutes to decades and length scales from centimeters to thousands of kilometers.

This article is concerned primarily with the physical processes causing time and space variability